Radiotherapy and Oncology 111 (2014) 354–359

Contents lists available at ScienceDirect

Radiotherapy and Oncology

journal homepage: www.thegreenjournal.com

Dose painting

Multi-modality functional image guided dose escalation in the presence of uncertainties

Markus Alber [a,*], Daniela Thorwarth [b]

[a] Department of Oncology, Aarhus University, Denmark; [b] Department for Radiation Oncology, Eberhard Karls University Tübingen, Germany

ARTICLE INFO

Article history:
Received 20 January 2014
Received in revised form 22 March 2014
Accepted 27 April 2014
Available online 28 May 2014

Keywords:
Functional imaging
MRI
PET
Dose painting
Prostate cancer
IMRT

ABSTRACT

Background and purpose: In order to increase local tumour control by radiotherapy without increasing toxicity, it appears promising to harness functional imaging (FI) to guide dose to sub-volumes of the target with a high tumour load and perhaps de-escalate dose to low risk volumes, in order to maximise the efficiency of the deposited radiation dose.

Methods and materials: A number of problems have to be solved to make focal dose escalation (FDE) efficient and safe: (1) how to combine ambiguous information from multiple imaging modalities; (2) how to take into account uncertainties of FI based tissue classification; (3) how to account for geometric uncertainties in treatment delivery; (4) how to add complementary FI modalities to an existing scheme. A generic optimisation concept addresses these points and is explicitly designed for clinical efficacy and for lowering the implementation threshold to FI-guided FDE. It combines classic tumour control probability modelling with a multi-variate logistic regression model of FI accuracy and an uncomplicated robust optimisation method.

Results: Its key elements are (1) that dose is deposited optimally when it achieves equivalent expected effect everywhere in the target volume and (2) that one needs to cap the certainty about the absence of tumour anywhere in the target region. For illustration, an example of a PET/MR-guided FDE in prostate cancer is given.

Conclusions: FDE can be safeguarded against FI uncertainties, at the price of a limit on the sensible dose escalation.

Functional imaging modalities (FI), e.g. various magnetic resonance imaging techniques (MRI) or positron emission tomography (PET) with various tracers, are increasingly being linked to tumour physiology or shown to have predictive or prognostic value [1]. Prevalent local failure in some tumour entities forms the rationale for a focal escalation of radiation dose (FDE) which is under investigation in pioneering clinical trials [2–5]. When it comes to quantitative use of FI, image interpretation and – quality quickly become an issue. Reported values of sensitivity and specificity of the most promising FI are usually in the range of 0.7–0.8, despite a multitude of technical challenges that have been mastered to establish reproducibility [6–8]. Apart from the large influence of inter-patient heterogeneity, volumetric pathologic ground truth for quantitative validation is cumbersome to obtain, limited in sample size and fraught with uncertainties of its own [9]. The combination of multiple FIs can increase sensitivity and specificity to up to 0.9 [10,11], but leaves the question how multiple FI can be harnessed for FDE.

FI-guided FDE can be achieved via a binary prescription dose map [12]. For example, Korporaal et al. [13] derived a logistic regression model from expert image classification of dynamic contrast enhanced (DCE) computed tomography and established tumour classification in prostate by thresholding. Langer et al. [14] and Groenendaal et al. [9,10] combined multiple MRI modalities via a logistic regression model and obtained binary tumour maps for prostate cancer via thresholding. Both models were derived from expert readings, and only the latter was validated against pathology. In this rapidly growing field, new FI are developed so quickly that a quantitative, volumetric pathologic validation may not commonly be available for any combination of modalities, thus raising the question how individually validated modalities can be combined with benefit.

As an alternative to binary volumes, Oberhammer et al. [15] interpreted the result of a support vector regression model as a pointwise probability of tumour presence. Subsequently, the dose prescription was directly based on this 3D probability map,

* Corresponding author.
E-mail address: markus@hyperion-imrt.org (M. Alber).

http://dx.doi.org/10.1016/j.radonc.2014.04.016
0167-8140/

thereby obviating thresholds. This was also mentioned in [13]. Here, we combine the advantages of both concepts to suggest a solution to four practical problems in FI-guided FDE: (1) how to amalgamate the information from multiple imaging modalities; (2) how to take into account uncertainties of FI-based tissue classification; (3) how to account for geometric uncertainties in treatment delivery; (4) how to incorporate additional FI to an existing scheme without having to establish volumetric pathologic ground truth for every new modality in combination with the others.

The concept is exemplified by a prostate case, comprising Diffusion-Weighted Imaging (DWI), resulting in an Apparent Diffusion Coefficient Map (ADC), dynamic contrast enhanced (DCE) MRI, yielding the parameter K^{trans} and [^{18}F]-Choline PET, simultaneously acquired on a PET/MR scanner.

Methods and materials

Probability of tumour presence

Assume a set of n properly registered FIs with intensities $I_{1\ldots n}(x)$ in N image points x is given. We choose a multivariate logistic regression model. Let the probability of finding tumour in the location x

$$p(x) = \frac{1}{1+\exp(-\gamma_0 - \sum_{i=1}^{n}\gamma_i I_i(x))}. \tag{1}$$

The regression coefficients $\gamma_i,\ i = 0\ldots n$ need to be determined ideally from pathology, expert readings, a pattern of failure analysis, or using alternative strategies (see example case). Notice that the logistic regression model assumes that the FI are independent, which needs verification especially for some MRI methods. The detrimental effect of correlations can be dealt with as presented in 'Derivation of odds from image intensity'.

For the following, it is helpful to review the alternative formulation of the logistic regression function in terms of the odds R_i:

$$p(x) = \frac{1}{1+\prod_{i=1}^{n} R_i(I_i(x))}. \tag{2}$$

In other words, if the image intensity $I(x)$ is found in point x, it is $R(I)$ times more likely to find *no* tumour there than to find any. Perfect certainty of tumour presence equals $R = 0$, while certainty about tumour absence is asymptotically approached if $R \to \infty$. In the case of volumes where p is small, a good approximation to Eq. (2) can be found

$$\log(p) = -\log\left(1+\prod_{i=1}^{n} R_i\right) \lesssim -\sum_{i=1}^{n}\log R_i \tag{3}$$

that illustrates how and with which weighting individual imaging modalities contribute independently to the local probability of tumour presence.

Maximizing tumour control in the presence of imaging uncertainties

The most commonly used measure for success in radiotherapy is the tumour control *probability* Q, i.e. treatment quality is measured in terms of a *high likelihood* of achieving the desired result. We extend this concept by the classification probability p, assuming that the tumour control probability $q(D(x))$ at dose $D(x)$ in point x is independent of its neighbours [16]. We find

$$Q = \prod_x ([1-p(x)] + [p(x)q(x)]), \tag{4}$$

where the first term is the tumour control when the point is indeed free of tumour and the second term the tumour control by the treatment else. For the purposes of dose optimisation, it is beneficial to choose $-\log(Q)$ as a cost function [17]. We find

$$-\log(Q) = -\sum_x \log\left(1-p(x)(1-q(x))\right) \tag{5}$$

$$\approx \sum_x p(x)(1-q(x)) \tag{6}$$

by a Taylor expansion of $\log(1-\epsilon) \approx -\epsilon$. Notice that in the context of dose optimisation, we can restrict ourselves to the situation of doses yielding reasonable tumour control, in other words the probability of failed cell kill $1-q(x)$ is typically in the order of 10^{-2} cm^{-3}. It is frequently expressed as $1-q = C\exp(-\alpha D-\beta D^2)$ with some cell-density-dependent constant C. Thus, the tumour presence probability $p(x)$ acts like a local cost function density weight, which is in keeping with its interpretation as a probability of a systematic classification error (see discussion). With the right calibration of C, the cost function becomes the expected number of surviving tumour cells given the uncertainty about their presence.

Accounting for systematic and random treatment uncertainties

The probability of tumour presence $p(x)$ is defined in the *patient* coordinate system. For treatment planning, the patient coordinate system has to be aligned with the *treatment* coordinate system. Naturally, the treatment plan and therefore also the optimum dose are defined relative to the treatment coordinate system. Random errors (with probability distribution $T(x,x')$) and systematic errors (with probability distribution $S(x,x')$) displace the points of the patient coordinate system relative to the treatment coordinate system. The effect of random errors, especially in a treatment with many fractions and a deep-seated target, is an averaging of the dose delivered to point x, which can be dealt with at several levels of approximation, depending on the target location. For the example below, we choose the dose convolution approach [18,19] which is appropriate if a random error does not affect the dose in the treatment coordinate system.

Systematic errors lead to an uncertainty about the classification of a point x at a location x' in the treatment coordinate system. For cost functions of the type of Eq. (5), a coverage probability $s(x')$ can be computed [20–23]:

$$s(x') = \int S(x,x')dx. \tag{7}$$

The cost function for the target in treatment coordinate system then reads

$$F = -\log(Q) = C\sum_{x'}\left(\int p(x)S(x,x')dx\right)\exp(-\alpha D(x')), \tag{8}$$

where the constant C could be dropped for convenience. For simplicity of the following argument, the fraction size dependence of the linear-quadratic-formalism has also been omitted. The integral $\tilde{p} = \int p(x)S(x,x')dx$ is the composite classification probability originating from FI interpretation uncertainty and systematic patient geometry errors in dose planning. Coverage probability can be applied to other cost functions such as equivalent uniform dose (EUD) or DVH penalties analogously.

Derivation of odds from image intensity

For clarity of argument, we start with

$$F = C\sum_x p(x)\exp(-\alpha D(x))$$

$$= C\sum_x \exp\left(-\alpha\left(D(x) - \frac{1}{\alpha}\log(p(x))\right)\right). \tag{9}$$

The optimum dose distribution $D^*(x)$ is required to employ the deposited energy with maximum efficiency for cell kill. This amounts to the requirement that the derivative with respect to D of all terms of the sum is equal in all points x, i.e. an additional dose

deposition causes the same expected additonal cell kill in all points. We introduce the nominal prescription dose D_{presc} to certain ($p = 1$) tumour locations and find

$$-\alpha C \exp(-\alpha D_{presc}) = -\alpha C \exp\left(-\alpha\left(D^*(x) - \frac{1}{\alpha}\log(p(x))\right)\right). \quad (10)$$

Thus,

$$D^*(x) = D_{presc} + \frac{1}{\alpha}\log(p(x))) \quad (11)$$

$$\lesssim D_{presc} - \frac{1}{\alpha}\sum_{i=1}^{n}\log R_i(x). \quad (12)$$

This inequality is illustrative if some or all FI indicate that a point is likely tumour-free, i.e. at least some of the odds R_i are large. Each FI allows a dose reduction to a likely tumour-free point proportionally to the logarithm of the odds, which amounts to relatively little. For example, assume a FI indicates a minimum probability of tumour of $p_{min} = 0.25$, equalling $R = 3$, or a possible dose reduction by 4 Gy if $\alpha = 0.28\ \mathrm{Gy}^{-1}$. The worst-case scenario of multiple FI having high odds in one point (all predict no tumour presence), but not being independent, leads to the composite odds $\prod_{i=1}^{n} R_i$ being overestimated. This can be prevented by introducing a maximum $R_{i,max}$ for the individual and R_{max} for the composite odds.

An estimate of p_{min} can be obtained from the published sensitivity s of the FI in question. In principle, $1 - p_{min}$ equals the negative predictive value. However, the latter depends on prevalence, in our case: the fraction of the target organ occupied by tumour cells. Since this quantity is hard to obtain and highly variable in a population, we assume that the prevalence is 0.5, which results in $p_{min} \leqslant 1 - s$. For typical sensitivities $s = 0.75$ for single modalities and $s = 0.9$ for combined modalities, the limits of $R_{i,max} = 3$ and $R_{max} = 9$, respectively, can be obtained. From this follows that the maximum safe dose reduction equals 8 Gy for $\alpha = 0.28\ \mathrm{Gy}^{-1}$ and 15 Gy for $\alpha = 0.15\ \mathrm{Gy}^{-1}$. Notice that by equating the minimum tumour classification $p_{min} = 1 - s$, we force the tumour classification model to be as imprecise for every individual patient as the diagnostic model is for a population. In other words, a diagnostic classification model can be absolutely certain about tumour absence, but this assessment can be wrong with probability $1 - s$. The modification we suggest makes the model only certain up to the residual chance p_{min} that tumour is absent.

We now address the inclusion of a new FI into an already existing setup, ideally without having to test the combination first, assuming each FI is validated independently. Observe that within the logistic regression model, the log-odds are a linear function by definition. With the maximum odds established above, we find:

$$\log R = \begin{cases} \log R_{i,max} & I \leqslant I_{low} \\ \log R_{i,max}/(I_{med} - I_{low})(I_{med} - I) & I > I_{low}. \end{cases} \quad (13)$$

With the choice of $R_{i,max}$, two more parameters suffice to define the calibration from image intensities to log-odds (see Fig. 1): the image intensity I_{med}, where the image is perfectly ambiguous ($R = 1$), and the intensity I_{low} where the signal suggests absence of tumour.[1] Notice, that the dose prescription depends more sensitively on R_{max} than on the other two parameters. Expressed in the parameters of Eq. (1), we find for the individual contribution to γ_0, $\gamma_{0,i} = -\log R_{i,max} I_{med}/(I_{med} - I_{low})$ and $\gamma_i = \log R_{max}/(I_{med} - I_{low})$.

Example

The example is an 80 y.o. prostate cancer patient who was examined prior to radiotherapy with combined PET/MR (Biograph mMR, Siemens Healthcare, Erlangen, Germany) using [^{18}F]-Choline as a PET tracer. After a fast series of diagnostic MR scans, DCE- as well as DWI/ADC-MR sequences were applied according to [9] to obtain maps of K^{trans} and ADC. The K^{trans} map was normalised [10]. This was part of an image validation study, within which each patient received a clinically indicated PET/CT. PET/MR images were obtained directly after PET/CT imaging with no additional tracer injection. PET/MR acquisition started 58 min after the injection of a total choline dose of 591 MBq. For treatment planning purposes, combined PET/MR data were rigidly matched to CT.

For image calibration, i.e. determination of regression factors γ_i for ADC and K^{trans}, two approaches were employed. Both rely on the data in [10], where the population averaged intensities for ADC and K^{trans} are given for suggestive and non-suggestive volumes. We choose I_{low} to be equal to the mean intensity of the non-suggestive volumes, and I_{med} to be the average between the suggestive and the non-suggestive. For method 1, we then fix the maximum individual odds $R_{i,max} = 3$, and compute γ_i. For method 2, we use the published regression factor γ_i and compute the corresponding maximum odds. All values are shown in Table 1. In addition to these MR images, Choline-PET was added following method 1.

Each FI can produce a classification probability separately, or in combination with others. To see the effect of adding modalities, Fig. 2 shows histograms of the voxelwise classification probability for the example patient. A more trusted single modality covers a wider range of classification probabilities. The effect of combining modalities is typically that the range of probabilities is stretched and the histogram becomes more bi-modal (the classification becomes more definitive). The histogram would only become less bi-modal if two modalities contradict each other. An unspecific modality would result in a horizontal shift. Of note, the two methods become more similar when both MRI-FI are used for classification. In the example, K^{trans} alone does not discriminate strongly between suggestive and non-suggestive points, while ADC alone is quite effective. The low specificity of Choline-PET can be read from the broad and not very peaked distribution.

Tumour classification probability maps are shown in Fig. 3: MRI-only by method 1 in Fig. 3a, MRI-only by method 2 in Fig. 3b, MRI + PET by method 1 in Fig. 3c, and MRI + PET convolved with the coverage probability kernel in Fig. 3d. The coverage probability kernel had a Gaussian shape with a width of 4σ and $\sigma = 3$ mm, 5 mm, and 4 mm in lateral, anterior-posterior and cranio-caudal directions, respectively.

Dose optimisation was performed with a number of physical and EUD-based dose constraints that were determined by creating a homogeneous 78 Gy treatment to the entire PTV, for delivery as a conventional 15 MV rotational IMRT ($\alpha = 0.25\ \mathrm{Gy}^{-1}$). With the same constraints, plans were generated for a nominal prescription dose D^* to the tumour foci of 95 Gy, equivalent to the FLAME trial [24]. The cost function Eq. (5) has no built-in limit for FDE so that an additional limit has to be formulated. For sufficient freedom to distribute the excess dose of the FDE, we limit the total deposited energy to the same amount as delivered for the homogeneous

Table 1
Parameters for the logistic regression model of the probability of local tumour presence. Parameters in **bold** obtain from the other parameters that are either derived from [10] or fixed by convention.

FI-calibration	R_{max}	I_{low}	I_{med}	γ	p_{min}
ADC-1	3	$1.47 \cdot 10^{-3}$	$1.18 \cdot 10^{-3}$	$3.8 \cdot 10^{3}$	0.25
ADC-2	**3.2**	$1.47 \cdot 10^{-3}$	$1.18 \cdot 10^{-3}$	$4.0 \cdot 10^{3}$	**0.24**
K^{trans}-1	3	1.19	1.62	**2.55**	0.25
K^{trans}-2	**2.3**	1.19	1.62	1.9	**0.30**
PET-1	3	1.0	1.5	**2.2**	0.25

[1] The formula is given for a PET-like signal: more intensity means higher presence of the quality of interest. The I-axis reverses for example for MRI-ADC.

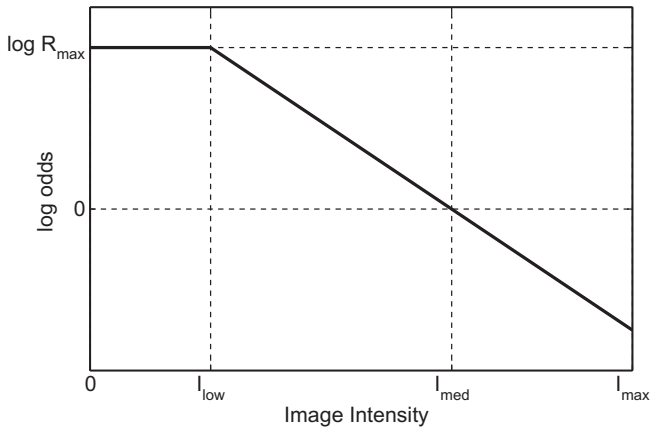

Fig. 1. Schematic illustration of the calibration of log-odds from image intensities. R_{max} is the maximum odds for the absence of tumour where the image intensity is at I_{low}, e.g. SUV = 1 for a PET image. I_{med} is the image intensity that corresponds to a 50:50 chance of finding tumour, i.e. an odds of 1.

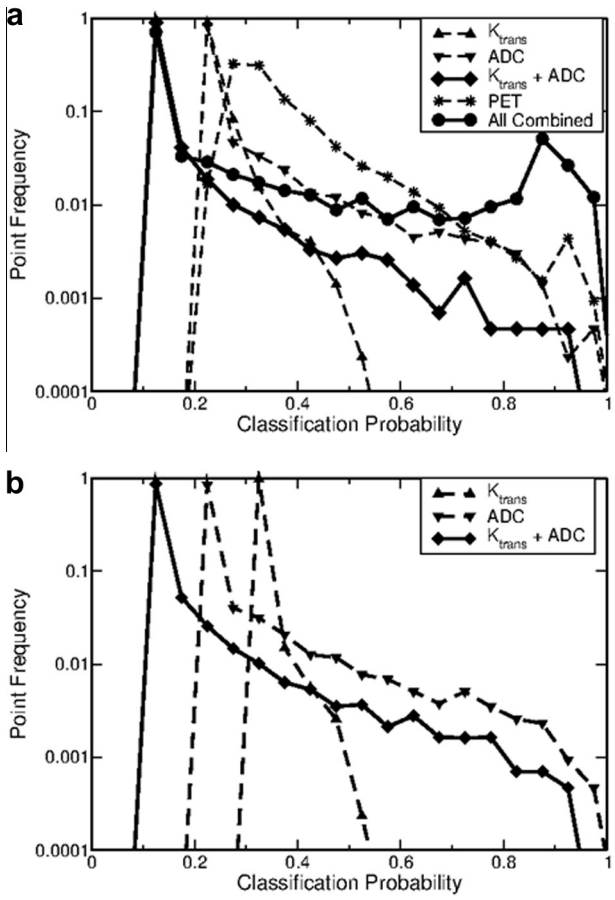

Fig. 2. Histograms of tumour classification probabilities for the semi-heuristic (top) and model-fit (bottom) method for single image modalities and their combinations.

78 Gy treatment. Fig. 3e and f show the treatment plans for the semi-heuristic MRI + PET and the model-fit MRI-only prescriptions.

Discussion

The presented method translates uncertainties in FI tumour classification and treatment delivery into a prescription for FDE. It embodies the economic rationale that dose should be equally effective everywhere. The resulting dose prescription function resembles "dose painting by numbers" (DPBN) [25,26], but its rationale is entirely different. Here, we want to deliver a uniform dose to all tumour foci, but the uncertainty about tumour presence results in a lower expected benefit of dose in potentially tumour-free points. It is illustrative to think of it as image-guided de-escalation in low risk volumes. If the volume was homogeneously classified as tumour, the ideal dose would be homogeneous. In contrast, DPBN directs dose according to its efficacy in a biologically heterogeneous tumour; therefore, the ideal dose is not uniform. By virtue of the assumption of equal limiting benefit in Eq. (10), both concepts could be combined by making the constants α, C dependent on x [27]. However, this requires that an (possibly additional) imaging modality correlates with a tumour quality, such as cell sensitivity, and not simply tumour presence, as in this framework.

We employ a continuous classification function from which volumes like a "low risk CTV", "high risk CTV" and "GTV" could be obtained by thresholding [10,13]. By using a continuous risk scale for dose prescription, these additional threshold parameters can be omitted. The logistic classification function is linear both in each single FI intensity and between multiple FIs. The latter allows us to expand existing imaging schemes with additional modalities easily. While a precise calibration of the classification function appears indispensable from a diagnostic accuracy point of view, it is the logarithm of the function that enters the dose prescription. Errors in the classification probability of suggestive volumes do not matter much ($\Delta D^* = -1/\alpha \log(p = 1 - \epsilon) \approx \epsilon/\alpha$). However, errors in the classification probability of non-suggestive volumes are amplified. To safeguard against erroneous dose de-escalation, a minimum probability of tumour presence, or maximum odds R_{max}, were introduced. Because of this modification, the model parameters can also be obtained from a practical heuristic. This is particularly important if some FI modalities have been tested individually, but not in combination. The quality of the test should be reflected in the choice of $R_{i,max}$. We consider $p_{min} = 0.25$, $R_{i,max} = 3$ for individual and $p_{min} = 0.1$, $R_{max} = 9$ for combined modalities generally cautiously optimistic. With these limits, the dose spread between tumour foci and low-risk volumes turns out to be in the range of 10–15 Gy. Larger spreads could only be justified if the imaging sensitivity for some combination of modalities exceeds 90%, or other effects like hypoxia contributed to a lower radiation sensitivity in larger foci. Especially in the context of the example, FI may indicate a higher Gleason score and thereby justify a greater spread.

The example dose plans were chosen to illustrate the effect of complementary image information on the dose prescription. For the MRI-only prescription, the tumour classification probability anywhere in the volume was slightly higher, and this translates into an approximately 1–3 Gy greater dose to the non-suggestive volume. The tumour focus appears better defined in the MRI + PET case, which results in a larger boost volume. An additional FI can increase the certainty about tumour absence and therefore justify a greater dose spread. Multiple FIs also dilute the effect of errors in a single image (see Eq. (11)). The relatively shallow prescription dose gradients pose no problem for modern IMRT delivery. It must be noted that functional imaging is still subject to a large operator variability and further efforts are necessary to establish inter-institutional consistency of data derived from functional imaging.

Alternative classification functions have been suggested, e.g. support vector machines [15,28,29], pattern recognition [30], and statistical methods [31–33]. Still, none of the more sophisticated methods offers a significantly better accuracy, reflecting that functional imaging is often a gaze into a rather dull crystal ball, clouded by inter-patient heterogeneity, image resolution and contrast, registration errors and non-specificity. We consider it crucial that any

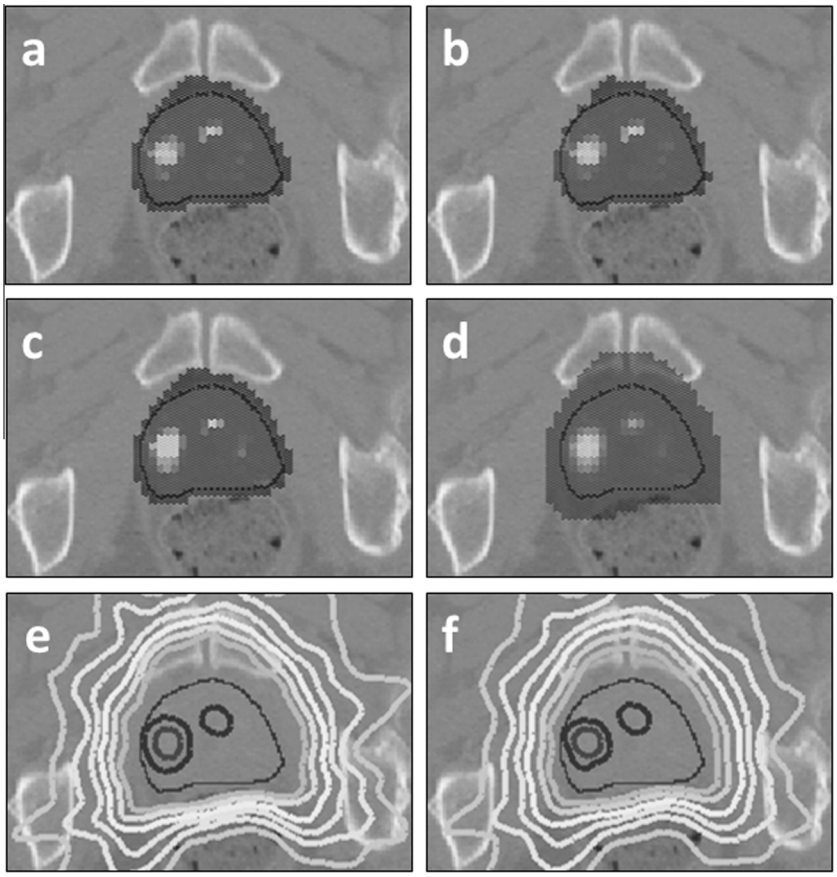

Fig. 3. Top row: raw tumour classification probability p for MRI-only obtained from the semi-heuristic method 1 and a model parameter fit (method 2) (a, b). Middle row: raw tumour classification probability p for MRI + PET obtained from the semi-heuristic method 1 (c) and the corresponding $\tilde{p}$ enhanced by coverage probability (d). Bottom row: dose distributions for the prescription map of (MRI + PET) x coverage probability (e) and for MRI x coverage probability (e). The high probability in the centre of the prostate is a MR-artefact caused by the urethra, which is dampened by the addition of PET. It was not removed for illustration purposes, to demonstrate the classification probability dependent dose levels.

alternative model also be safeguarded with a lower limit on the probability of tumour presence.

The standard approach to deal with treatment-related uncertainties is the expansion of the target volume by a margin. Technically, this could be approximated by the convolution of the classification map with a box function on an ellipsoid $S_{box}(x, x')$. While this will expand the suggestive volume in the classification map, it will not change the structure of Eq. (8). As an alternative, we suggest to employ a 3D-Gaussian (or similar) error distribution that incorporates the coverage probability distributions of systematic treatment errors, which yields a more focussed and specific dose prescription map. It is also a template for dealing with image registration uncertainties between the FI modalities and the planning CT image. We suggest that each modality be blurred with the relevant systematic uncertainty distribution *before* they are blended together by the logistic regression model. This also leads to some next-neighbour correlations that improve the model accuracy, as suggested by Groenendaal et al. [10]. Intriguingly, coverage probability can be understood as the classification uncertainty of a point in the treatment room as being occupied by tumour, caused by systematic patient geometry changes. The concept of $\tilde{p}$ proposed here expands this by the equally systematic uncertainty of target volume identification. It yields the most efficient dose distribution on average in a patient population, where the average runs over the unknown systematic errors in image classification. Although the approach guarantees that best use is made of the total deposited energy in a population, some patients will receive a worse-than-average treatment, whose risk can only be controlled by realistic expectations about the power of functional imaging.

Conclusions

Functional image guided dose escalation can be safeguarded against functional imaging uncertainties, at the price of a limit on the sensible dose escalation.

Conflicts of interest statement

None declared.

Acknowledgements

This work was supported by CIRRO – The Lundbeck Foundation Center for Interventional Research in Radiation Oncology and The Danish Council for Strategic Research. A part of the research has received funding from the European Research Council under the European Union's Seventh Framework Programme (FP/2007-2013)/ERC Starting Grant Agreement No. 335367. The authors thank Arndt-Christian Müller, Nina Schwenzer and Holger Schmidt (Department of Diagnostic and Interventional Radiology, Tübingen) for PET/MR acquisition.

References

[1] Balter J, Haffty B, Dunnick N, Siegel E, Palta J, Hahn S, et al. Imaging opportunities in radiation oncology. Int J Radiat Oncol Biol Phys 2011;79:342–7.

[2] Lips I, van der Heide U, Haustermans K, van Lin E, Pos F, Franken S et al. Single blind randomised phase III trial to investigate the benefit of a focal lesion ablative microboost in prostate cancer (flame-trial): study protocol for a randomised controlled trial. Trials 12, 2010.

[3] van Elmpt W, De Ruysscher D, van der Salm A, Lakeman A, van der Stoep J, Emans D, et al. The PET-boost randomised phase II dose-escalation trial in non-small cell lung cancer. Radiother Oncol 2012;104:67–71.

[4] Duprez F, De Neve W, De Gersem W, Coghe M, Madani I. Adaptive dose painting by numbers for head-and-neck cancer. Int J Radiat Oncol Biol Phys 2011;80:1045–55.

[5] Leclerc M, Maingon P, Hamoir M, Dalban C, Calais G, Nuyts S, et al. A dose escalation study with intensity modulated radiation therapy (IMRT) in T2N0, T2N1, T3N0 squamous cell carcinomas (SCC) of the oropharynx, larynx and hypopharynx using a simultaneous integrated boost (SIB) approach. Radiother Oncol 2013;106:333–40.

[6] Groenendaal G, van den Berg CAT, Korporaal JG, Philippens M, Luijten PR, van Vulpen M, et al. Simultaneous MRI diffusion and perfusion imaging for tumour delineation in prostate cancer patients. Radiother Oncol 2010;95:185–90.

[7] van der Heide U, Houweling A, Groenendaal G, Beets-Tan R, Lambin P. Functional MRI for radiotherapy dose painting. Magn Reson Imaging 2012;30:1216–23.

[8] Boellaard R, O'Doherty M, Weber W, Mottaghy F, Lonsdale M, Stroobants S, et al. FDG PET and PET/CT: EANM procedure guidelines for tumour PET imaging: version 1.0. Eur J Nucl Med Mol Imaging 2010;37:181–200.

[9] Groenendaal G, Moman MR, Korporaal JG, van Diest PJ, van Vulpen M, Philippens M, et al. Validation of functional imaging with pathology for tumour delineation in the prostate. Radiother Oncol 2010;94:145–50.

[10] Groenendaal G, Borren A, Moman MR, Monninkhof E, van Diest PJ, Philippens M, et al. Pathologic validation of a model based on diffusion-weighted imaging and dynamic contrast-enhanced magnetic resonance imaging for tumour delineation in the prostate peripheral zone. Int J Radiat Oncol Biol Phys 2012;82:537–44.

[11] Van den Bergh L, Koole M, Isebaert S, Joniau S, Deroose C, Oyen R, et al. Is there an additional value of ^{11}C-choline PET-CT to T2-weighted MRI images in the localisation of intraprostatic tumour nodules? Int J Radiat Oncol Biol Phys 2012;83:1486–92.

[12] Thorwarth D, Geets X, Paiusco M. Physical radiotherapy treatment planning based on functional PET/CT data. Radiother Oncol 2010;96:317–24.

[13] Korporaal J, van den Berg C, Groenendaal G, Moman M, van Vulpen M, van der Heide U. The use of probability maps to deal with the uncertainties in prostate cancer delineation. Radiother Oncol 2010;94:168–72.

[14] Langer D, van der Kwast T, Evans A, Trachtenberg J, Wilson B, Haider M. Prostate cancer detection with multi-parametric MRI: logistic regression analysis of quantitative T2, diffusion-weighted imaging, and dynamic contrast-enhanced MRI. J Magn Res Imaging 2009;30:327–34.

[15] Oberhammer P, Gröger A, Schlemmer H, Ganswindt U, Belka C, Alber M. Inclusion of uncertainties in multiparametric MR imaging into dose painting for prostate tumours. Radiother Oncol 2009;92:S75.

[16] Munro T, Gilbert C. The relation between tumour lethal doses and the radiosensitivity of tumour cells. Br J Radiol 1961;34:246–51.

[17] Alber M, Nüsslin F. An objective function for radiation treatment optimisation based on local biological measures. Phys Med Biol 1999;44:479–93.

[18] Beckham WA, Keall PJ, Siebers JV. A fluence-convolution method to calculate radiation therapy dose distributions that incorporate random set-up error. Phys Med Biol 2002;47:3465–73.

[19] Chetty IJ, Rosu M, Tyagi N, Marsh LH, McShan DL, Balter JM, et al. A fluence convolution method to account for respiratory motion in three-dimensional dose calculations of the liver: a Monte-Carlo study. Med Phys 2003;30:1776–80.

[20] Stroom JC, de Boer HCJ, Huizenga H, Visser AG. Inclusion of geometrical uncertainties in radiotherapy treatment planning by means of coverage probability. Int J Radiat Biol Phys 1999;43:905–19.

[21] Baum C, Alber M, Birkner M, Nüsslin F. Robust treatment planning for intensity modulated radiotherapy of prostate cancer based on coverage probabilities. Radiother Oncol 2006;78:27–35.

[22] Sir M, Pollock S, Epelman M, Lam K, Ten Haken R. Ideal spatial radiotherapy dose distributions subject to positional uncertainties. Phys Med Biol 2006;51:6329–47.

[23] Witte M, van der Geer J, Schneider C, Lebesque J, Alber M, van Herk M. IMRT optimisation including random and systematic geometric errors based on the expectation of TCP and NTCP. Med Phys 2007;34:3544–55.

[24] ClinicalTrials.gov, Flame: investigate the benefit of a focal lesion ablative microboost in prostate cancer. <www.ClinicalTrials.gov>.

[25] Bentzen S. Theragnostic imaging for radiation oncology: dose-painting by numbers. Lancet Oncol 2005;6:112–7.

[26] Thorwarth D, Eschmann S, Paulsen F, Alber M. Hypoxia dose painting by numbers: a planning study. Int J Radiat Oncol Biol Phys 2007;68:291–300.

[27] Alber M, Paulsen F, Eschmann S, Machulla H. On biologically conformal boost dose optimisation. Phys Med Biol 2003;48:N31–5.

[28] Vos P, Hambrock T, Hulsbergen-van de Kaa C, Futterer J, Barentsz J, Huisman H. Computerised analysis of prostate lesions in the peripheral zone using dynamic contrast enhanced MRI. Med Phys 2008;35:888–99.

[29] Artan Y, Haider M, Langer D, van der Kwast T, Evans A, Yang Y, et al. Prostate cancer localisation with multispectral MRI using cost-sensitive support vector machines and conditional random fields. IEEE Trans Image Process 2010;19:2444–55.

[30] Kelm BM, Menze BH, Zechmann CM, Baudendistel KT, Hamprecht FA. Automated estimation of tumour probability in prostate magnetic resonance spectroscopic imaging: pattern recognition vs quantification. Magn Reson Med 2007;57:150–9.

[31] Chan I, Wells III WM, Mulkern RV, Haker S, Zhang J, Zou KH, et al. Detection of prostate cancer by integration of line-scan diffusion, T2-mapping and T2-weighted magnetic resonance imaging; a multichannel statistical classifier. Med Phys 2003;30:2390–8.

[32] Liu X, Langer D, Haider M, Yang Y, Wernick M, Yetik I. Prostate cancer segmentation with simultaneous estimation of Markov random field parameters and class. IEEE Trans Med Imaging 2009;28:906–15.

[33] Ozer S, Langer D, Liu X, Haider M, van der Kwast T, Evans A, et al. Supervised and unsupervised methods for prostate cancer segmentation with multispectral MRI. Med Phys 2010;37:1873–83.